Totally asymmetric exclusion process on chains with a double-chain section in the middle: Computer simulations and a simple theory

Jordan Brankov,* Nina Pesheva, and Nadezhda Bunzarova
Institute of Mechanics, Bulgarian Academy of Sciences, Academician G. Bonchev Street 4, 1113 Sofia, Bulgaria
(Received 19 December 2003; published 16 June 2004)

Computer simulations of the totally asymmetric simple-exclusion process on chains with a double-chain section in the middle are performed in the case of random-sequential update. The outer ends of the chain segments connected to the middle double-chain section are open, so that particles are injected at the left end with rate α and removed at the right end with rate β. At the branching point of the graph (the left end of the middle section) the particles choose with equal probability $1/2$ which branch to take and then simultaneous motion of the particles along the two branches is simulated. With the aid of a simple theory, neglecting correlations at the junctions of the chain segments, the possible phase structures of the model are clarified. Density profiles and nearest-neighbor correlations in the steady states of the model at representative points of the phase diagram are obtained and discussed. Cross correlations are found to exist between equivalent sites of the branches of the middle section whenever they are in a coexistence phase.

DOI: 10.1103/PhysRevE.69.066128 PACS number(s): 02.50.Ey, 05.60.−k, 05.70.Ln, 64.60.Ht

I. INTRODUCTION

The one-dimensional asymmetric simple-exclusion process (ASEP) is one of the simplest models of self-driven many-particle systems with particle conserving continuous-time stochastic dynamics. The process, first introduced in Refs. [1,2], has been extensively studied in simple chains with periodic, closed, and open boundary conditions. In the latter case, when particles are injected at the left end with rate α and removed at the right end with rate β, boundary-induced phase transitions have been predicted [3]. Exact results have been obtained for the steady-state properties under different updating rules: random-sequential [4–6], forward- and backward-ordered sequential [7,8], sublattice-parallel [9,10], and fully parallel [11,12]; see also Ref. [13]. The case of random-sequential update has been considered on a ring with a defect ("slow") bond [14] and with a moving impurity (a single "negative" particle) [15]. In both cases the particle-density profile was found to develop a shock structure. Multispecies generalizations have been suggested, too [16,17].

One of the natural physical interpretations of the totally asymmetric version of ASEP (TASEP) is given in terms of a single-lane vehicular traffic, see the recent reviews [18,19]. However, the fully parallel dynamics is considered as most appropriate for traffic modeling, and it is laid on the basis of more sophisticated update rules [20,21]. The TASEP with parallel update results in the Nagel-Schreckenberg model [20] with maximum vehicle velocity $v_{\max}=1$.

Recently much attention has been paid to cellular automaton models of traffic on roads with localized inhomogeneities modeling on- and off-ramps [22–24]. Such spatial inhomogeneities were shown to lead to different dynamical phases of congested traffic. Microscopic models of multilane traffic with different lane-changing rules have been suggested and studied, too, see Ref. [25] and references therein. Two-dimensional versions of the TASEP have been used to model traffic in a city, see, e.g., Refs. [26–28] for the case of periodic boundary conditions and Refs. [29,30] for open boundaries. Recently, the anisotropy effect of the probabilities of changing the direction of motion of the cars on the dynamical jamming transition under both periodic and open boundaries has been studied [31]. In the two-dimensional lattice models, however, the motion of the up-directed and right-directed cars is controlled by traffic lights. Similarly, in the multilane traffic models some mandatory rules for lane changes are specified. Such studies of complicated road networks are necessary for better understanding of real traffic. To the best of our knowledge, the case of bifurcation or junction of equivalent roads has not yet been considered.

In this paper we attempt to model traffic flow on a road network consisting of a single lane with a double-chain section in the middle. In other words, we consider a single-lane road which bifurcates into two equivalent branches which subsequently merge again into a single lane. Due to the network complexity, we choose the simplest model of the vehicular motion in terms of TASEP with random-sequential update, since this update is the easiest for analytical treatment. In particular, the exact expression for the current includes only nearest-neighbor correlations. By neglecting these correlations at the junctions of the simple-chain segments, we introduce in our simple theory effective injection and removal rates for each chain segment and study the possible phase structures of the whole system in terms of these rates. Moreover, the nearest-neighbor correlations can be readily evaluated in our computer simulations which, in turn, allows us to distinguish between finite-size effects and correlation ones. One would expect the same principal results to hold for the other types of update, since, e.g., the phase diagram of the TASEP has the same basic structure for all the updates. The two branches of the middle section are assumed to be equivalent simple chains consisting of a large number of sites, and so are the simple chains connected to them, see Fig. 1. The ends of the chain segments are open, so that

*Electronic address: brankov@bas.bg

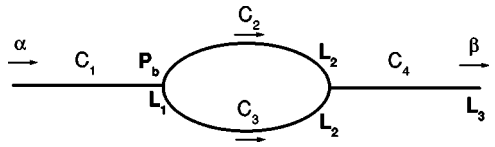

FIG. 1. Schematic representation of the model system: one-dimensional chain with a double-chain section in the middle. The particles are injected at the left end with probability α and removed at the right end with probability β. The head (C_1) and tail (C_4) chain segments consist of L_1 and L_3 sites, respectively, and the chain segments C_2, C_3 of the middle section consist of equal number of sites L_2. At the bifurcation point the particles take the upper branch with probability p_b. In the simulations we set $L_1=L_2=L_3=L$ and $P_b=1/2$.

particles are injected at the outer left end with rate α and removed at the outer right end with rate β. At the branching point of the graph the particles choose with equal probability $1/2$ which branch of the middle double-chain section to take. To simulate simultaneous motion of the vehicles along the two branches, each trial to move a particle on one of them is immediately followed by a trial to move a particle on the other branch. If a particle occupying the last site of a branch is chosen to move, and the site to the right, at which the branches merge, is empty, then that particle hops to the latter site, thus blocking (temporarily) the flow from the other branch. One may ask the question: will the presence of an additional lane in the middle increase the flow through the entire network? In favor of the negative answer is the argument that the total flow is limited by the bulk capacity of chain segments connected to the middle double-chain section. On the other hand, the exact solution of the single-chain problem [4,5] shows that the flow depends on the phase of the chain under consideration which, in turn, depends on the input and output rates at its left end and right end, respectively. Here we recall that the branching and merging points can be viewed as inhomogeneities of the entire network which are expected to produce correlations between the occupation numbers of the nearby sites. Due to the constancy of the current through the bonds of each chain segment, these correlations change the density profile near the ends of the chains. Thus, the presence of a double-chain section in between two simple chains affects the output rate of the chain to the left and the input rate of the chain to the right. Hence, the answer to the above question is not so obvious.

By means of computer simulations we have evaluated the steady-state current, density profiles, nearest-neighbor correlations along the simple-chain segments, as well as the cross correlations between equally positioned sites on the two branches of the middle section.

II. THE MODEL

In the present paper we study TASEP on a graph consisting of a simple chain with a double-chain section in the middle. A schematic representation of the system is shown in Fig. 1. The system has four distinct parts: a head chain segment C_1 of L_1 sites $i=1,2,\ldots,L_1$, a middle section consisting of upper, C_2, and lower, C_3, branches of L_2 sites each, and a tail chain segment C_4 of L_3 sites $i=L_1+L_2+1, L_1+L_2+2,\ldots,L_1+L_2+L_3$. To simplify notation, we denote by $L_{\mathrm{tot}}=L_1+L_2+L_3$ the total number of sites a particle can pass through. Due to the hard-core exclusion each site can be empty or occupied by at most one particle, i.e., $\tau_i=\{0,1\}$, respectively, where τ_i is the random occupation number of site i; the occupation numbers of the branches of the middle section will be distinguished by the superscripts (1) and (2) for the upper $\tau_i^{(1)}$, and lower $\tau_i^{(2)}$ branch, respectively. The open boundary conditions are implemented by introducing an extra "source" site $i=0$ to the left of site $i=1$, which plays the role of a reservoir of particles. The time evolution of the system obeys the random-sequential update. At each time step $t\to t+1$, a pseudorandom number is drawn from the set $\{0,1,\ldots,L_{\mathrm{tot}}\}$ with equal probability $1/(L_{\mathrm{tot}}+1)$. If the integer i is in the bulk, particles jump to the neighboring right-hand site with probability $p=1$, provided the target site is empty:

$$\tau_i(t+1)=\tau_i(t)\tau_{i+1}(t),$$

$$\tau_{i+1}(t+1)=\tau_{i+1}(t)+[1-\tau_{i+1}(t)]\tau_i(t). \qquad (1)$$

If $i=0$ is chosen and $\tau_1=0$, then a particle is injected at site $i=1$ with probability α, otherwise the configuration remains unchanged. If the last site $i=L_{\mathrm{tot}}$ of the tail chain is chosen and if it is occupied by a particle, then that particle is removed from the system with probability β, otherwise the configuration remains unchanged. These boundary conditions imply that the system is coupled to reservoirs of particles with constant densities α and $1-\beta$, respectively.

The last site $i=L_1$ of the head chain is a branching point from which the particles can take the upper or the lower branch of the double-chain middle section with equal probability $P_b=1/2$. The simulation of simultaneous and independent traffic of particles on the two branches is performed in the following way. Whenever a site i belonging to the middle section is chosen, i.e., when $L_1+1\leqslant i\leqslant L_1+L_2$, with probability $1/2$ that site is taken in the upper or lower branch and the rule (1) is applied to it first. Then a second site j, $L_1+1\leqslant j\leqslant L_1+L_2$, is chosen randomly from the other branch of the middle section and the rule (1) is applied to it next. The particles from both the upper and lower branches of the middle section can enter the first site $i=L_1+L_2+1$ of the tail chain of the system whenever it is empty. In the present study we consider only the case when all chain segments have equal number of sites, i.e., $L_1=L_2=L_3=L$.

III. PRELIMINARY ANALYSIS

To systematically study the steady-state properties of our network, one has to select representative values of the input α and output β rates. For sufficiently large L, the natural guidelines are given by the exact results known for the simple chain with open boundaries in the thermodynamic limit [5,6]. Let us recall briefly that in the bulk limit the simple chain is in the low-density phase $\mathcal{L}$ when $\alpha<\beta,\alpha\leqslant 1/2$, it is in the high density phase $\mathcal{H}$ when $\alpha>\beta,\beta\leqslant 1/2$, it is in the maximum-current phase $\mathcal{M}$ when

$\alpha>1/2, \beta>1/2$, and it is on the coexistence line $\mathcal{C}$ between the low-density and high-density phases when $\alpha=\beta, \alpha<1/2$. Thus, we start by assuming that each of the different chain segments C_i, $i=1,2,3,4$, of our model is expected to develop steady-state properties characteristic of one of the above simple-chain phases. It is now convenient to denote the expected phase structure of our model by a string of three letters $(\mathcal{X}_1,\mathcal{X}_{2,3},\mathcal{X}_4)$, with $\mathcal{X}_i \in \{\mathcal{L},\mathcal{H},\mathcal{M},\mathcal{C}\}$, $i=1,\ldots,4$. Here $\mathcal{X}_i$ stands for the phase of the chain segment C_i, and $\mathcal{X}_2=\mathcal{X}_3$ due to the equivalence of the upper (C_2) and lower (C_3) branches of the middle section. Of course, not all the possible combinations are allowed to occur, e.g., due to the fact that the current through the branches of the middle section is half the one through the head and tail chains, for macroscopic chains these branches may never be found in the maximum-current phase. We shall refine the possible phase structure of our model at two successive levels A and B.

A. First-level analysis

At the first level A we take into account only the exact results for a simple chain with open boundaries in the thermodynamic limit. In this case, the pair correlations between nearest-neighbor sites vanish in the bulk and the current $J(\rho)$ through a chain with bulk particle density ρ is given by $J(\rho)=\rho(1-\rho)$. Denote by ρ_i the bulk density in the chain segment C_i, and by $\langle\tau_i\rangle$ the steady-state particle density at site i. Then, taking into account the inflow $J_{\text{in}}=\alpha(1-\langle\tau_1\rangle)$ and outflow $J_{\text{out}}=\beta\langle\tau_{L_{\text{tot}}}\rangle$ of the system, the current conservation in our model implies the chain of equalities:

$$J=\alpha(1-\langle\tau_1\rangle)=\rho_1(1-\rho_1)=2\rho_{2,3}(1-\rho_{2,3})=\rho_4(1-\rho_4)=\beta\langle\tau_{L_{\text{tot}}}\rangle. \tag{2}$$

Here we have taken into account that each of the middle-section branches is chosen with probability $P_b=1/2$ which, together with $L_2=L_3$, leads to their equivalence, hence $\rho_2=\rho_3$. Thus, we obtain that the bulk densities must obey the relations

$$\rho_1=\begin{cases}\rho_4,\\ 1-\rho_4,\end{cases}\qquad \rho_2=\rho_3=\frac{1}{2}\{1\pm[1-2\rho_1(1-\rho_1)]^{1/2}\}. \tag{3}$$

Let us confine our consideration now to the determination of the allowed phase structures consisting of the pure phases $\mathcal{L}$, $\mathcal{H}$, and $\mathcal{M}$ only. At that we shall keep in mind that when, under given values of the rates α and β, a chain segment may be in both a low- and high-density phase, it may occur as well on the coexistence line $\mathcal{C}$ between these two phases. Consider now all the pure phases of the head chain C_1.

A1. Let the head chain C_1 be in the low-density phase $(\mathcal{X}_1=\mathcal{L})$ with bulk density $\rho_1<1/2$. Then, from the exact solution for a single chain we have

$$J=\alpha(1-\alpha),\quad \langle\tau_1\rangle=\alpha,\quad \rho_1=\alpha<1/2. \tag{4}$$

Note that Eq. (3) allows the tail chain C_4 to be either in $\mathcal{L}$ with $\rho_4=\alpha$, or in $\mathcal{H}$ with $\rho_4=1-\alpha$. The latter case, $\mathcal{X}_4=\mathcal{H}$, implies $\beta<1/2$ and $J=\beta(1-\beta)$, which is possible only if $\alpha=\beta$. Since the current through each of the branches of the middle section equals half the total one, $\rho_{2,3}(1-\rho_{2,3})=\alpha(1-\alpha)/2$, C_2 and C_3 may be found either in $\mathcal{L}$ with $\rho_{2,3}^{-}(\alpha)<\alpha$ or in $\mathcal{H}$ with $\rho_{2,3}^{+}(\alpha)>1-\alpha$, where

$$\rho_{2,3}^{\pm}(\alpha)=\tfrac{1}{2}\{1\pm[1-2\alpha(1-\alpha)]^{1/2}\}. \tag{5}$$

Thus, the possible pure-phase structures with $\mathcal{H}_1=\mathcal{L}$ are

$$(\mathcal{L},\mathcal{L},\mathcal{L}),\quad (\mathcal{L},\mathcal{H},\mathcal{L})\quad \text{if } \alpha<1/2, \alpha\neq\beta \tag{6}$$

and

$$(\mathcal{L},\mathcal{L},\mathcal{H}),\quad (\mathcal{L},\mathcal{H},\mathcal{H})\quad \text{if } \alpha=\beta<1/2. \tag{7}$$

A2. Let the head chain C_1 be in the high-density phase $(\mathcal{X}_1=\mathcal{H})$ with bulk density $\rho_1>1/2$. Then, from Eq. (3) we obtain that the tail chain C_4 can be either in $\mathcal{L}$ with $\rho_4=1-\rho_1$ or in $\mathcal{H}$ with $\rho_4=\rho_1$. In the former case the phase structure is

$$(\mathcal{H},\mathcal{L},\mathcal{L}),\quad (\mathcal{H},\mathcal{H},\mathcal{L}), \tag{8}$$

and no further conclusions can be drawn.

In the latter case, $\mathcal{X}_4=\mathcal{H}$ implies

$$\beta<1/2,\quad J=\beta(1-\beta),\quad \rho_1=\rho_4=\langle\tau_{L_{\text{tot}}}\rangle=1-\beta>1/2. \tag{9}$$

Since the current through each of the branches of the middle section equals half the total one, $\rho_{2,3}(1-\rho_{2,3})=\beta(1-\beta)/2$, C_2 and C_3 can be found in $\mathcal{L}$ with $\rho_{2,3}^{-}(\beta)<1-\rho_1$, or in $\mathcal{H}$ with $\rho_{2,3}^{+}(\beta)>\rho_1$, where $\rho_{2,3}^{\pm}(\beta)$ is given by Eq. (5). Thus, the other two possible pure-phase structures with $\mathcal{X}_1=\mathcal{H}$ are

$$(\mathcal{H},\mathcal{L},\mathcal{H}),\quad (\mathcal{H},\mathcal{H},\mathcal{H})\quad \text{if } \beta<1/2. \tag{10}$$

A3. Let the head chain C_1 be in the maximum-current phase $(\mathcal{X}_1=\mathcal{M})$, which may happen if $\alpha>1/2$. Then $J=1/4$ and Eq. (3) implies that $\rho_1=\rho_4=1/2$, hence the tail chain C_4 must also be in the maximum-current phase, $\mathcal{X}_4=\mathcal{M}$, which may happen if $\beta>1/2$. Since the current through each of the branches of the middle section equals $1/8$, C_2 and C_3 can be found either in $\mathcal{L}$ with $\rho_{2,3}^{-}<1/2$, or in $\mathcal{H}$ with $\rho_{2,3}^{+}>1/2$, where

$$\rho_{2,3}^{\pm}=(1\pm 1/\sqrt{2})/2. \tag{11}$$

Thus, the possible pure-phase structures with $\mathcal{X}_1=\mathcal{M}$ are

$$(\mathcal{M},\mathcal{L},\mathcal{M}),\quad (\mathcal{M},\mathcal{H},\mathcal{M})\quad \text{if } \alpha>1/2 \text{ and } \beta>1/2. \tag{12}$$

From the above analysis it is evident that a little information can be inferred about the phase structure of our model from the current conservation condition (2). That is why, at the next level approximation B we shall ignore the correlations between the chain segments, which will make possible the definition of effective injection and/or removal rates at the junctions of the simple chains. On the one hand, this is an approximation, since the inhomogeneities introduced by the branching and merging nodes are expected to induce correlations, as is the case of a simple chain, or a ring, with a

defect bond, or a single-impurity particle, respectively. On the other hand, the comparison of the so obtained predictions with the results of computer simulations will reveal in which cases the correlations between the chain segments are essential for the phase structure of our network.

B. Second-level analysis

Passing to the second level B, we assume the following pairs of random variables to be independent: τ_{L_1} and $\tau^{(1,2)}_{L_1+1}$, as well as $\tau^{(1,2)}_{L_1+L_2}$ and $\tau_{L_1+L_2+1}$. The neglect of the corresponding pair correlations leads to the approximate expressions for the total current:

$$J \simeq \tfrac{1}{2}\langle\tau_{L_1}\rangle(1-\langle\tau^{(1)}_{L_1+1}\rangle)+\tfrac{1}{2}\langle\tau_{L_1}\rangle(1-\langle\tau^{(2)}_{L_1+1}\rangle) \simeq (\langle\tau^{(1)}_{L_1+L_2}\rangle+\langle\tau^{(2)}_{L_1+L_2}\rangle)(1-\langle\tau_{L_1+L_2+1}\rangle). \quad (13)$$

Hence, by comparing with the case of a simple chain with open boundaries, and taking into account the equivalence of the two branches of the middle section, we obtain estimates for the removal rate β_1 of the head chain C_1, the injection $\alpha_{2,3}$, and removal $\beta_{2,3}$ rates of the chain segments $C_{2,3}$, and the injection rate α_4 of the tail chain C_4:

$$\beta_1 = 1-\langle\tau^{(1,2)}_{L_1+1}\rangle, \quad \alpha_{2,3}=\tfrac{1}{2}\langle\tau_{L_1}\rangle, \quad \beta_{2,3}=1-\langle\tau_{L_1+L_2+1}\rangle, \quad \alpha_4 = 2\langle\tau^{(1,2)}_{L_1+L_2}\rangle. \quad (14)$$

On the grounds of the above assumptions, we are in the position to reconsider in more detail the theoretical expectations about the phase structure of our model.

B1. Consider first the phase structures given in Eq. (6), where $\mathcal{X}_1=\mathcal{L}$ implies $\alpha<1/2$ and $\alpha<\beta_1$, $\mathcal{X}_4=\mathcal{L}$ implies $\alpha_4<1/2$ and $\alpha_4<\beta$. Then, from Eqs. (2) and (14) it follows that

$$\alpha_4=\alpha<1/2, \quad J=\alpha(1-\alpha), \quad \rho_1=\rho_4=\langle\tau_{L_1+L_2+1}\rangle=\alpha, \quad \beta_{2,3}=1-\alpha. \quad (15)$$

The above relations are compatible only with $\mathcal{X}_{2,3}=\mathcal{L}$ when the simple-chain solution yields

$$\langle\tau^{(1,2)}_{L_1+1}\rangle=\rho_{2,3}=\alpha_{2,3}, \quad \beta_1=1-\langle\tau^{(1,2)}_{L_1+1}\rangle=1-\alpha_{2,3}. \quad (16)$$

Hence, taking into account Eq. (3) with $\rho_1=\alpha$, and keeping in mind that in the low-density phase $\rho_{2,3}<1/2$, we obtain

$$\alpha_{2,3}=\rho^-_{2,3}(\alpha)<\beta_{2,3}=1-\alpha, \quad \beta_1=1-\rho^-_{2,3}(\alpha)=\rho^+_{2,3}(\alpha)>\alpha. \quad (17)$$

The above equations prove that the phase structure $(\mathcal{L},\mathcal{L},\mathcal{L})$ is compatible with the conditions on the external rates $\alpha<1/2$ and $\alpha<\beta$, under which a single chain is in the low-density phase.

The alternative $\mathcal{X}_{2,3}=\mathcal{H}$ is excluded, since then one would have $\rho_{2,3}=1-\beta_{2,3}=\alpha$, hence, $\beta_{2,3}=1-\alpha>1/2$ violates the condition for a high-density phase of $C_{2,3}$.

Consider now the pure-phase structures given in Eq. (7), which are allowed under the condition $\alpha=\beta<1/2$. Recall that a single chain with such injection and removal rates would be on the coexistence line between low- and high-density phases. From $\mathcal{X}_1=\mathcal{L}$ and $\mathcal{X}_4=\mathcal{H}$, taking into account Eq. (14), we infer

$$\langle\tau_1\rangle=\rho_1=\alpha, \quad \langle\tau_{L_1}\rangle=\alpha(1-\alpha)/\beta_1, \quad \alpha_{2,3}=\alpha(1-\alpha)/(2\beta_1) \quad (18)$$

and

$$\langle\tau_{L_1+L_2+1}\rangle=1-\alpha(1-\alpha)/\alpha_4, \quad \langle\tau_{L_{\rm tot}}\rangle=\rho_4=1-\alpha, \quad \beta_{2,3}=\alpha(1-\alpha)/\alpha_4. \quad (19)$$

When $\mathcal{X}_{2,3}=\mathcal{L}$ we obtain from Eq. (3) that $\rho_{2,3}=\rho^-_{2,3}(\alpha)$, and from the simple-chain solution it follows that

$$\langle\tau^{(1,2)}_{L_1+1}\rangle=\rho^-_{2,3}(\alpha)=\alpha_{2,3}=\langle\tau_{L_1}\rangle/2, \quad \langle\tau^{(1,2)}_{L_1+L_2}\rangle=\alpha_{2,3}(1-\alpha_{2,3})/\beta_{2,3}=\alpha_4/2. \quad (20)$$

The above equalities determine $\alpha_{2,3}=\rho^-_{2,3}(\alpha)<1/2$ and from Eq. (14) we find also $\beta_1=1-\alpha_{2,3}=\rho^+_{2,3}(\alpha)>\alpha$. The latter inequality, together with $\alpha<1/2$, ensures that $\mathcal{X}_1=\mathcal{L}$. However, the values of $\beta_{2,3}$ and α_4 remain undefined, only a relation between them exists according to the last equality in Eq. (19). The conditions $\beta_{2,3}>\alpha_{2,3}$ for $\mathcal{X}_{2,3}=\mathcal{L}$ and $\alpha_4>\beta=\alpha$ for $\mathcal{X}_4=\mathcal{H}$ can be rewritten in terms of the local density $\langle\tau^{(1,2)}_{L_1+L_2}\rangle$ as

$$\alpha/2<\langle\tau^{(1,2)}_{L_1+L_2}\rangle<\rho^+_{2,3}(\alpha)=1-\langle\tau^{(1,2)}_{L_1+1}\rangle. \quad (21)$$

When $\mathcal{X}_{2,3}=\mathcal{H}$ we obtain from Eq. (3) that $\rho_{2,3}=\rho^+_{2,3}(\alpha)$, and from the simple-chain solution it follows that

$$\langle\tau^{(1,2)}_{L_1+L_2}\rangle=\rho^+_{2,3}(\alpha)=1-\beta_{2,3}=\langle\tau_{L_1+L_2+1}\rangle, \quad \langle\tau^{(1,2)}_{L_1+1}\rangle=1-\beta_{2,3}(1-\beta_{2,3})/\alpha_{2,3}=1-\beta_1. \quad (22)$$

The above equalities determine $\beta_{2,3}=\rho^-_{2,3}(\alpha)<1/2$ and from Eq. (14) we find also $\alpha_4=2\rho^+_{2,3}(\alpha)>2\alpha$. The latter inequality, together with $\beta=\alpha<1/2$, ensures that $\mathcal{X}_4=\mathcal{H}$. However, the values of β_1 and $\alpha_{2,3}$ remain undefined, only a relation between them, namely, $\alpha_{2,3}=\alpha(1-\alpha)/(2\beta_1)$ follows from the second equalities in Eqs. (14) and (18). The conditions $\alpha<\beta_1$ for $\mathcal{X}_1=\mathcal{L}$ and $\beta_{2,3}<\alpha_{2,3}$ for $\mathcal{X}_{2,3}=\mathcal{H}$ can be rewritten in terms of the local density $\langle\tau^{(1,2)}_{L_1+1}\rangle$ as

$$\rho^-_{2,3}(\alpha)<\langle\tau^{(1,2)}_{L_1+1}\rangle<1-\alpha. \quad (23)$$

Here we have taken into account that, due to Eqs. (18) and (19), $\beta_{2,3}<\alpha_{2,3}$ is equivalent to $\alpha_4>\beta_1/2$.

Next, from Eqs. (18) and (19) it follows that if $\beta_1=\alpha_4$, then $\alpha_{2,3}=\beta_{2,3}=\rho^-_{2,3}(\alpha)<1/2$, which implies that the chain segments of the middle section are on the coexistence line $\mathcal{C}$ between the phases with bulk densities $\rho^-_{2,3}(\alpha)$ and $\rho^+_{2,3}(\alpha)$. From the simple-chain solution we know that the local density profile is then linear, with

$$\langle\tau^{(1,2)}_{L_1+1}\rangle=\rho^-_{2,3}(\alpha), \quad \langle\tau^{(1,2)}_{L_1+L_2}\rangle=\rho^+_{2,3}(\alpha). \quad (24)$$

Summarizing the above results, we obtain the following possibilities:

$$(\mathcal{L},\mathcal{L},\mathcal{L}) \text{ if } \alpha<1/2 \text{ and } \alpha<\beta, \tag{25}$$

$$(\mathcal{L},\mathcal{L},\mathcal{H}) \text{ if } \alpha=\beta<1/2 \text{ and } \alpha/2<\langle\tau^{(1,2)}_{L_1+L_2}\rangle<\rho^{+}_{2,3}(\alpha), \tag{26}$$

$$(\mathcal{L},\mathcal{H},\mathcal{H}) \text{ if } \alpha=\beta<1/2 \text{ and } \rho^{-}_{2,3}(\alpha)<\langle\tau^{(1,2)}_{L_1+1}\rangle<1-\alpha, \tag{27}$$

$$(\mathcal{L},\mathcal{C},\mathcal{H}) \text{ if } \alpha=\beta<1/2 \text{ and } \langle\tau^{(1,2)}_{L_1+1}\rangle=\rho^{-}_{2,3}(\alpha)=1-\langle\tau^{(1,2)}_{L_1+L_2}\rangle. \tag{28}$$

B2. Consider next the phase structures given in Eq. (8). Due to the simple-chain solution, $\mathcal{X}_1=\mathcal{H}$ implies

$$\beta_1<1/2,\ \alpha>\beta_1,\ \rho_1=1-\beta_1>1/2,\ J=\beta_1(1-\beta_1),\ \langle\tau_{L_1}\rangle=1-\beta_1, \tag{29}$$

and $\mathcal{X}_4=\mathcal{L}$ implies

$$\alpha_4<1/2,\ \alpha_4<\beta,\ \rho_4=\alpha_4,\ J=\alpha_4(1-\alpha_4),\ \langle\tau_{L_1+L_2+1}\rangle=\alpha_4. \tag{30}$$

Hence, taking into account Eq. (2), we obtain

$$\alpha_4=\beta_1,\ \rho_{2,3}=\rho^{-}_{2,3}(\beta_1)<1/2,\ \rho_4=1-\rho_1=\beta_1<1/2. \tag{31}$$

In addition, from Eq. (14) we obtain

$$\langle\tau^{(1,2)}_{L_1+1}\rangle=1-\beta_1=\langle\tau_{L_1}\rangle=2\alpha_{2,3}>1/2,\quad \langle\tau^{(1,2)}_{L_1+L_2}\rangle=\alpha_4/2=\beta_1/2<1/4. \tag{32}$$

One can readily see that the above relations are incompatible with both possibilities $\mathcal{X}_{2,3}=\mathcal{L}$ and $\mathcal{X}_{2,3}=\mathcal{H}$. Indeed, in the former case the simple-chain solution yields

$$\langle\tau^{(1,2)}_{L_1+1}\rangle=\rho^{-}_{2,3}(\beta_1)=\alpha_{2,3}<1/2, \tag{33}$$

which contradicts the first chain of equalities in Eq. (32), since $1-\beta_1\neq 2\rho^{-}_{2,3}(\beta_1)$ for all $\beta_1\neq 1$. In the latter case, $\mathcal{X}_{2,3}=\mathcal{H}$, the simple-chain solution yields

$$\langle\tau^{(1,2)}_{L_1+L_2}\rangle=\rho^{+}_{2,3}(\beta_1)>1/2, \tag{34}$$

which contradicts the second chain of equalities in Eq. (32), since $2\rho^{+}_{2,3}(\beta_1)\neq\beta_1$ for all β_1. Therefore, phase structures of the type $(\mathcal{H},\mathcal{X},\mathcal{L})$ are excluded by our analysis.

Consider now the pure-phase structures given in Eq. (10). From Eqs. (9) and (29), which hold true in this case, it follows that $\beta=\beta_1<1/2$ and $\langle\tau_{L_1}\rangle=1-\beta>1/2$. The possibility $\mathcal{X}_{2,3}=\mathcal{L}$ is excluded, since then the single-chain solution would give

$$\langle\tau^{(1,2)}_{L_1+1}\rangle=\rho^{-}_{2,3}(\beta)=\alpha_{2,3}, \tag{35}$$

which (for $\beta\neq 1$) contradicts the result that follows from Eq. (14) and the last equality in Eq. (29):

$$\alpha_{2,3}=\langle\tau_{L_1}\rangle/2=(1-\beta)/2. \tag{36}$$

It remains to consider the other possibility $\mathcal{X}_{2,3}=\mathcal{H}$ when the simple-chain solution gives

$$\langle\tau^{(1,2)}_{L_1+L_2}\rangle=\rho^{+}_{2,3}(\beta)=1-\beta_{2,3}, \tag{37}$$

hence $\beta_{2,3}=\rho^{-}_{2,3}(\beta)$. From Eq. (14) it follows that

$$\alpha_4=2\langle\tau^{(1,2)}_{L_1+L_2}\rangle=2(1-\beta_{2,3})=2\rho^{+}_{2,3}(\beta)>1, \tag{38}$$

which, together with $\beta<1/2$, ensures the condition $\alpha_4>\beta$ for $\mathcal{X}_{2,3}=\mathcal{H}$. From Eqs. (29) and (37) it follows that for all $\beta\neq 1$,

$$\alpha_{2,3}=\langle\tau_{L_1}\rangle/2=(1-\beta)/2>\beta_{2,3}=\rho^{-}_{2,3}(\beta) \text{ and } \beta_{2,3}=\rho^{-}_{2,3}(\beta)<1/2. \tag{39}$$

The above inequalities are the necessary and sufficient conditions for the chain segments $C_{2,3}$ of the middle section to be in the high-density phase. Thus, we have ended up with the phase structure

$$(\mathcal{H},\mathcal{H},\mathcal{H}) \text{ if } \alpha>\beta \text{ and } \beta<1/2. \tag{40}$$

B3. Finally, consider the phase structures given in Eq. (12). From the simple-chain solutions for $\mathcal{X}_1=\mathcal{M}$ (when $\alpha>1/2$ and $\beta_1>1/2$) and $\mathcal{X}_4=\mathcal{M}$ (when $\alpha_4>1/2$ and $\beta>1/2$) we have

$$\langle\tau_1\rangle=1-(4\alpha)^{-1}>1/2,\ \langle\tau_{L_1}\rangle=(4\beta_1)^{-1}<1/2,\quad \langle\tau_{L_1+L_2+1}\rangle=1-(4\alpha_4)^{-1}>1/2,\ \langle\tau_{L_{\text{tot}}}\rangle=(4\beta)^{-1}<1/2. \tag{41}$$

Hence, taking into account Eq. (14), we obtain $\alpha_{2,3}=1/(8\beta_1)<1/4$ and $\beta_{2,3}=1/(4\alpha_4)<1/2$.

If $\mathcal{X}_{2,3}=\mathcal{L}$, then $\rho_{2,3}=\rho^{-}_{2,3}$ and the simple-chain solution yields

$$\langle\tau^{(1,2)}_{L_1+1}\rangle=\alpha_{2,3}=\rho^{-}_{2,3}<1/4,\quad \langle\tau^{(1,2)}_{L_1+L_2}\rangle=\alpha_{2,3}(1-\alpha_{2,3})/\beta_{2,3}=\alpha_4/2. \tag{42}$$

With the aid of Eq. (14) we determine $\beta_1=\rho^{+}_{2,3}>1/2$, while $\beta_{2,3}$ and α_4 remain unknown. The remaining condition $\beta_{2,3}>\alpha_{2,3}$ for $\mathcal{X}_{2,3}=\mathcal{L}$ yields $\alpha_4<2\rho^{+}_{2,3}$. The latter inequality and the condition $\alpha_4>1/2$ for $\mathcal{X}_4=\mathcal{M}$ lead to

$$1/4<\langle\tau^{(1,2)}_{L_1+L_2}\rangle<\rho^{+}_{2,3}. \tag{43}$$

If the other possibility $\mathcal{X}_{2,3}=\mathcal{H}$ takes place, then $\rho_{2,3}=\rho^{+}_{2,3}$ and the simple-chain solution yields

$$\langle\tau^{(1,2)}_{L_1+L_2}\rangle=\rho^{+}_{2,3}=1-\beta_{2,3}=1-(4\alpha_4)^{-1},\quad \langle\tau^{(1,2)}_{L_1+1}\rangle=\beta_{2,3}(1-\beta_{2,3})/\alpha_{2,3}=1-\beta_1. \tag{44}$$

Hence, we obtain the results $\beta_{2,3}=\rho^{-}_{2,3}<1/2$ and α_4

$=2\rho_{2,3}^{+}>1$, which are in agreement with the assumed phases of $C_{2,3}$ and C_4. The remaining conditions $\alpha_{2,3}>\beta_{2,3}$ for $\mathcal{X}_{2,3}=\mathcal{H}$ and $\beta_1>1/2$ for $\mathcal{X}_1=\mathcal{M}$ lead to the inequalities $1/2<\beta_1<\rho_{2,3}^{+}$, or, equivalently,

$$\rho_{2,3}^{-}<\langle\tau_{L_1+1}^{(1,2)}\rangle<1/2. \tag{45}$$

Since the chain segments $C_{2,3}$ can be both in low-density and high-density pure phases, they may be found on the coexistence line, too. In this case the simple-chain solution yields a linear density profile with

$$\langle\tau_{L_1+1}^{(1,2)}\rangle=\rho_{2,3}^{-},\langle\tau_{L_1+L_2}^{(1,2)}\rangle=\rho_{2,3}^{+}. \tag{46}$$

Hence we obtain $\beta_1=\rho_{2,3}^{+}>1/2$, $\alpha_4=2\rho_{2,3}^{+}>1$, and $\alpha_{2,3}=\beta_{2,3}=\rho_{2,3}^{-}<1/4$, in full agreement with the assumed phases of all the chain segments.

Summarizing the above results, we obtain the following possibilities:

$$(\mathcal{M},\mathcal{L},\mathcal{M}) \text{ if } \alpha>1/2,\beta>1/2 \text{ and } 1/4<\langle\tau_{L_1+L_2}^{(1,2)}\rangle<\rho_{2,3}^{+}, \tag{47}$$

$$(\mathcal{M},\mathcal{H},\mathcal{M}) \text{ if } \alpha>1/2,\beta>1/2 \text{ and } \rho_{2,3}^{-}<\langle\tau_{L_1+1}^{(1,2)}\rangle<1/2, \tag{48}$$

$$(\mathcal{M},\mathcal{C},\mathcal{M}) \text{ if } \alpha>1/2,\beta>1/2 \text{ and } \langle\tau_{L_1+1}^{(1,2)}\rangle=\rho_{2,3}^{-}=1-\langle\tau_{L_1+L_2}^{(1,2)}\rangle. \tag{49}$$

Thus, the refined analysis of the allowed phase structures, based on the neglect of the pair correlations between the nearest-neighbor occupation numbers belonging to different chain segments, yields the eight possibilities given by Eqs. (25)–(28), (40), and (47)–(49). However, our computer simulations, presented in the following section, show that whenever the chain segments $C_{2,3}$ of the middle section may exist in either the low- or high-density phases, they are always found on the coexistence line. The numerical results for each of the remaining four phase structures will be compared with the predictions of our simple theory in the following section.

IV. SIMULATION RESULTS

The main results of our computer simulations are obtained for chain segments of equal number of sites $L=100$ or $L=200$. Time is measured in units of $(3L+1)$ local trials, which we call steps per site (SPS). Our estimates of the relaxation time N_τ for reaching the steady state from the empty initial configuration show that it may strongly depend on the phase structure of the system, as well as on the quantity under consideration: as a rule, the shortest relaxation times are found for the evolution the total density per site of a chain segment, and the longest for the local cross correlations between equivalent sites belonging to the two branches of the middle section. Below, we present the results for the different phase structures observed, along with a comparison with the theoretical predictions obtained in the preceding section.

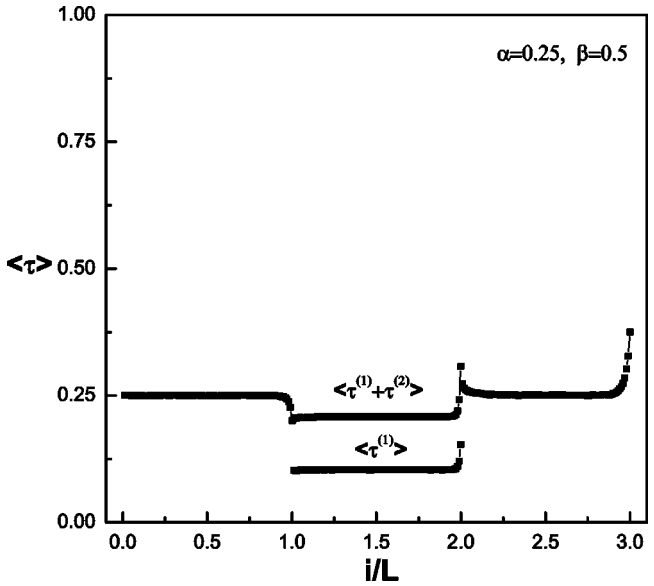

FIG. 2. The simulation results for the local density profile $\langle\tau\rangle$ in the system as function of the scaled distance $x=i/L$, $i=1,2,\ldots,3L$, in the low-density phase $(\mathcal{L},\mathcal{L},\mathcal{L})$ for the specific choice $\alpha=0.25,\beta=0.5$.

1. Case $\alpha<1/2$ and $\alpha<\beta$

This case was studied for the particular values of $\alpha=0.25$ and $\beta=0.5$. The estimated relaxation time for the bulk density is $N_\tau\simeq 400$ SPS. The steady-state quantities were evaluated on the basis of a twofold averaging over 300 independent runs of length 10^4 SPS each (after the omission of the first 5×10^3 SPS). The so obtained local density profile is shown in Fig. 2 as a function of the normalized coordinate $x=i/L$. As expected from our preliminary analysis, see Eq. (25), the phase structure $(\mathcal{L},\mathcal{L},\mathcal{L})$ is realized. The comparison of the theoretical predictions (with the superscript th) and the simulation results (with the superscript sim) for the current and the bulk densities in the simple-chain segments shows that they agree fairly well, within expected finite-size and finite-sample corrections:

$$J^{\text{th}}=0.1875,\ \rho_1^{\text{th}}=0.25,\ \rho_{2,3}^{\text{th}}=0.1047\ldots,\ \rho_4^{\text{th}}=0.25,$$

$$J^{\text{sim}}=0.1874(1),\ \rho_1^{\text{sim}}=0.2501(4),\ \rho_{2,3}^{\text{sim}}=0.104(1),\ \rho_4^{\text{sim}}=0.2513(6). \tag{50}$$

Even details of the shape of the density profiles are well explained. The density profile of the head chain segment C_1 is typical for a simple chain in the subregion $\alpha<1/2<\beta$ of the low-density phase, where $\alpha<1/2$ and $1-\beta_1<\alpha<\beta_1$. Indeed, the above conditions are fulfilled, since from Eq. (17) we have $\beta_1>\alpha$ and $1-\beta_1=\rho_{2,3}^{-}(0.25)=0.1047\ldots<\alpha$. Thus, the density profile is flat from the first site $i=1$ till close to the end site $i=L_1$, where it bends downward to reach the theoretical value given by Eqs. (14) and (17):

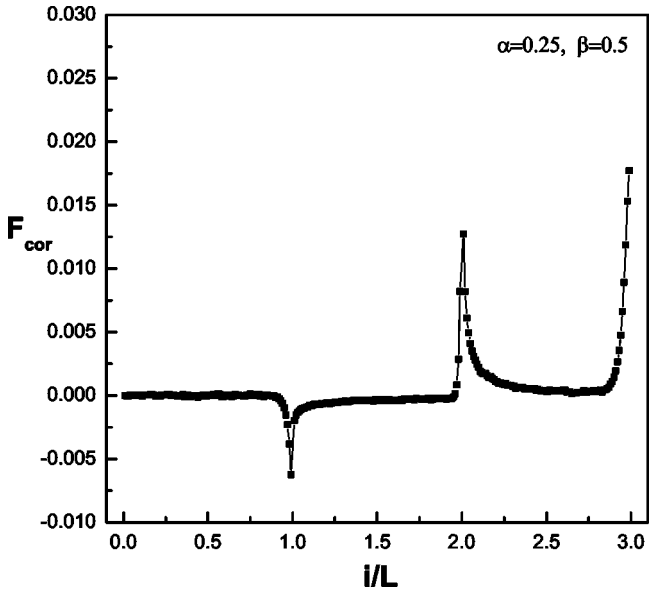

FIG. 3. The simulation results for the nearest-neighbor correlation function F_{cor} in the low-density phase $(\mathcal{L},\mathcal{L},\mathcal{L})$ for the specific choice $\alpha=0.25, \beta=0.5$.

$$\langle \tau_{L_1} \rangle^{\text{th}} = 2\alpha_{2,3} = 2\rho^{-}_{2,3}(0.25) = 0.2094\ldots\ . \tag{51}$$

The latter value is slightly higher than the simulation estimate $\langle \tau_{L_1} \rangle^{\text{sim}} \approx 0.2008$.

The local density profile of the chain segments $C_{2,3}$ of the middle section closely resembles the one of a simple chain in the subregion $\alpha<\beta<1/2$ of the low-density phase, where $\alpha_{2,3}<1/2$ and $\alpha_{2,3}<\beta_{2,3}<1-\alpha_{2,3}$. The above conditions hold, since from Eq. (17) we have $\alpha_{2,3}<\beta_{2,3}$ and $\alpha_{2,3}<1-\beta_{2,3}=\alpha$. As is seen from Fig. 2, the density profile is almost flat from the first site, where $\langle \tau_{L_1+1} \rangle^{\text{sim}} \approx 0.1023$ is just slightly less than the bulk value $\rho^{\text{th}}_{2,3}=0.1047\ldots$, till close to the end, where it bends upward to the value $\langle \tau^{(1,2)}_{L_1+L_2} \rangle^{\text{sim}} \approx 0.1536$. However, the latter value is noticeably higher than the theoretical prediction following from Eqs. (14) and (15):

$$\langle \tau^{(1,2)}_{L_1+L_2} \rangle^{\text{th}} = \alpha_4/2 = \alpha/2 = 0.125. \tag{52}$$

The observed discrepancies are obviously due to the short-range nearest-neighbor anticorrelations and correlations which appear near the inhomogeneities introduced by the bifurcation and merging points, see Fig. 3.

The local density profile of the tail chain segment C_4 has a slight bending upward close to the left end, where $\langle \tau_{L_1+L_2+1} \rangle^{\text{sim}} \approx 0.273$ is somewhat higher than the bulk density. This effect is apparently caused by the above mentioned correlations. Apart from it, the profile fits well to the one of a simple chain in the subregion $\alpha<\beta<1/2$ of the low-density phase, where $\alpha_4<1/2$ and $\alpha_4<\beta<1-\alpha_4$. The above conditions hold, since from Eq. (15) we have $\alpha_4=\alpha=0.25$ and, in the case under consideration $\beta=0.5$. As is seen from Fig. 2, the density profile is flat in the bulk and has a well pronounced bending upward close to the last site $i=L_{\text{tot}}$, where $\langle \tau_{L_{\text{tot}}} \rangle^{\text{sim}} \approx 0.3752$. The latter value is in remarkable agreement with the exact simple-chain solution in the thermodynamic limit:

$$\langle \tau_{L_{\text{tot}}} \rangle^{\text{th}} = \alpha_4(1-\alpha_4)/\beta = 0.375. \tag{53}$$

The observed discrepancies are obviously due to the short-range nearest-neighbor correlations which appear near the inhomogeneities introduced by the bifurcation and merging points, see Fig. 3.

2. Case $\alpha=\beta<1/2$

Most surprising are the results of our computer simulations in this case. For chain segments of length $L=200$ sites and the particular values $\alpha=\beta=0.25$ the estimated relaxation time is $N_\tau \approx 6\times 10^5$. The results reported here were obtained after averaging over 200 runs of length 2×10^6 SPS each. Since we have no control over the local densities $\langle \tau^{(1,2)}_{L_1+1} \rangle$ and $\langle \tau^{(1,2)}_{L_1+L_2} \rangle$, we cannot force the system in the phase structures given by Eqs. (26) and (27). Therefore, we expect to find the chain segments of the middle section on the coexistence line, see Eq. (28), between the low-density phase with bulk density $\rho^{-}_{2,3}(0.25) \approx 0.1047$ and the high-density phase with bulk density $\rho^{+}_{2,3}(0.25) \approx 0.8953$. However, the simulations yielded values of the local density at the ends of these segments,

$$\langle \tau^{(1,2)}_{L_1+1} \rangle^{\text{sim}} = 0.2395(1), \langle \tau^{(1,2)}_{L_1+L_2} \rangle^{\text{sim}} = 0.7503(1), \tag{54}$$

which are very different from the theoretical expectations, see Eq. (24).

Another unusual feature is the nonvanishing slope in the density profiles of the head and tail chain segments, see Fig. 4, which are expected to be in the low- and high-density phase, respectively. In excellent agreement with our simple theory are only the local densities at the first and the last sites of the system:

$$\langle \tau_1 \rangle^{\text{sim}} \approx 0.2508,\ \langle \tau_{L_{\text{tot}}} \rangle^{\text{sim}} \approx 0.7493. \tag{55}$$

According to Eqs. (18) and (19), the above values are to be compared to $\langle \tau_1 \rangle^{\text{th}}=0.25$ and $\langle \tau_{L_{\text{tot}}} \rangle^{\text{th}}=0.75$, respectively.

An inspection of the nearest-neighbor correlations shown in Fig. 5 reveals two important features. First, strong correlations with parabolic spatial dependence in the chain segments of the middle section, which is indicative of phase coexistence with completely delocalized domain wall between the low- and high-density phases. Second, rather strong correlations developing in the head and tail chain segments away from the open boundaries. The spatial dependence of these correlations resembles the wings of a parabola with missing central part. In an attempt to explain these features, we elaborate the model of completely delocalized domain wall by taking into account the inhomogeneous block structure of our system.

Let the position of the domain wall y be a continuous random variable taking values in the interval $(0,3L)$. Suppose that it is distributed with uniform density over each of the chain segments. Take into account that the domain wall in C_1 and C_4 is different from that in the branches of the

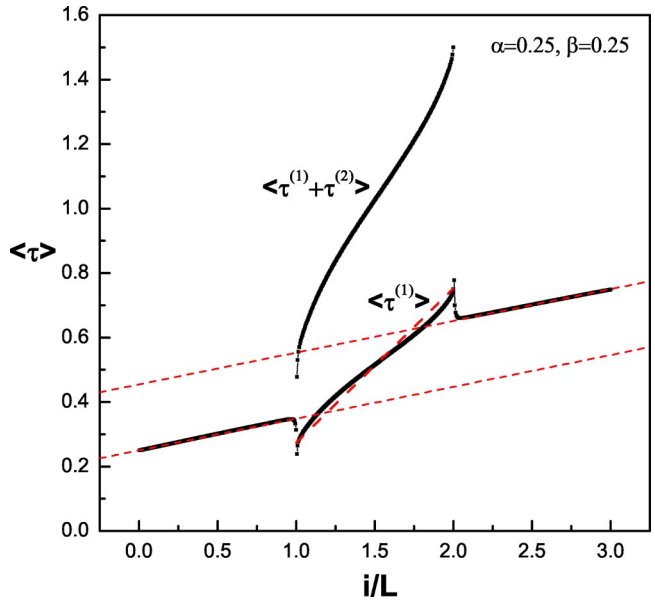

FIG. 4. (Color online) The simulation results for the averaged density profile $\langle\tau\rangle$ in the system as function of the scaled distance $x=i/L$, $i=1,2,\ldots,3L$, at the phase point $\alpha=0.25,\beta=0.25$ (solid squares) and the analytic results given by Eq. (58) (dashed lines).

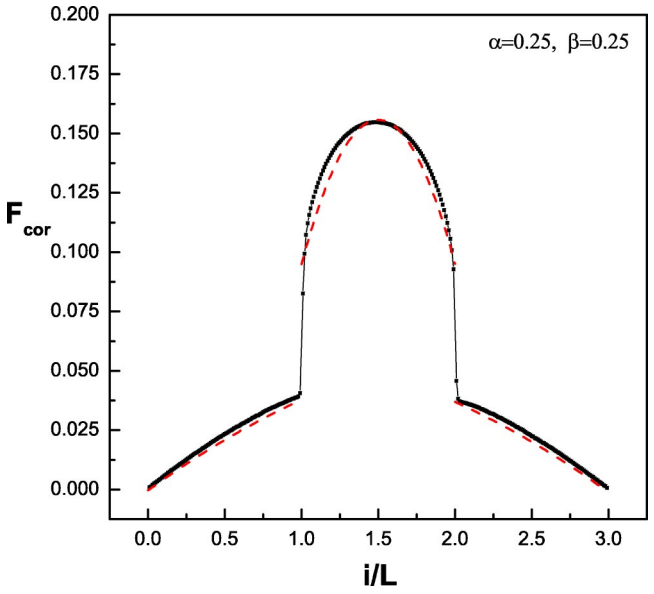

FIG. 5. (Color online) The simulation results for the nearest-neighbor correlation function F_{cor} at the phase point $\alpha=0.25,\beta=0.25$ (solid squares—solid line), and the analytic results given by Eq. (61) (dashed lines).

middle section $C_{2,3}$. Indeed, the current through both C_1 and C_4 is equal to $J=\alpha(1-\alpha)$, hence the domain wall in each of these segments is between a low-density phase with bulk density $\rho_1=\alpha<1/2$ and a high-density phase with bulk density $\rho_4=1-\alpha>1/2$. On the other hand, the current through each of the chain segments C_2 and C_3 of the middle section is equal to $J/2=\alpha(1-\alpha)/2$, and the domain wall in each of these segments is between a low-density phase with bulk density $\rho^-_{2,3}(\alpha)$ and a high-density phase with bulk density $\rho^+_{2,3}(\alpha)$. Therefore, these domain walls are expected to travel with different velocities, due to which the probability p_1 of finding the domain wall in the head or tail chains may differ from the probability p_2 of finding it in the middle section. Let us denote by $P(\cdot)$ the probability of the event in the brackets and pass to spatial coordinates normalized by L, namely, $x=i/L$ and $\xi=y/L$. Then we can write the probability distribution function of the domain wall in the form

$$P(\xi<x)=\begin{cases}p_1x & \text{if } 0<x<1\\ p_1+p_2(x-1) & \text{if } 1<x<2\\ p_1+p_2+p_1(x-2) & \text{if } 2<x<3,\end{cases} \tag{56}$$

where $2p_1+p_2=1$, since $P(\xi<3)=1$. Since the density profile is given by the general expression

$$\langle\tau(x)\rangle=\begin{cases}(1-\alpha)P(\xi<x)+\alpha P(\xi>x) & \text{if } 0<x<1\\ \rho^+_{2,3}(\alpha)P(\xi<x)+\rho^-_{2,3}(\alpha)P(\xi>x) & \text{if } 1<x<2\\ (1-\alpha)P(\xi<x)+\alpha P(\xi>x) & \text{if } 2<x<3\end{cases} \tag{57}$$

by taking into account that $p_2=1-2p_1$, we obtain explicitly

$$\langle\tau(x)\rangle=\begin{cases}\alpha+(1-2\alpha)p_1x & \text{if } 0<x<1\\ \rho^-_{2,3}(\alpha)+[\rho^+_{2,3}(\alpha)-\rho^-_{2,3}(\alpha)][p_1+(1-2p_1)(x-1)] & \text{if } 1<x<2\\ (1-\alpha)(1-p_1)+\alpha p_1+(1-2\alpha)p_1(x-2) & \text{if } 2<x<3.\end{cases} \tag{58}$$

The following important consequences from the above theoretical model agree quantitatively with the simulation results. First, the density profiles of all the chain segments are linear, but have different slopes: $(1-2\alpha)p_1$ for C_1 and C_4, and $[1-2\alpha(1-\alpha)]^{1/2}(1-2p_1)$ for $C_{2,3}$. In our case of $\alpha=0.25$, the evaluation of p_1 from the linear approximation to the density profiles of C_1 and C_4 yields $p_1\approx0.197$. This, in turn, gives us the estimate 0.479 for the slope of the density profiles of the segments $C_{2,3}$ of the middle section, which agrees well enough with the simulation result shown in Fig. 4. Second, the evaluation of the local densities at the internal ends of the chain segments, based on Eq. (58), yields

$$\langle \tau_{L_1} \rangle^{\rm th} \approx 0.348,\ \langle \tau_{L_1+1}^{(1,2)} \rangle^{\rm th} \approx 0.260,$$
$$\langle \tau_{L_1+L_2}^{(1,2)} \rangle^{\rm th} \approx 0.7395,\ \langle \tau_{L_1+L_2+1} \rangle^{\rm th} \approx 0.6515. \tag{59}$$

In spite of the improved agreement with the simulation results in some cases, the discrepancies remain rather large. An explanation of this fact can be looked for in the correlations that develop at the junctions of the head and tail chains with the double-chain middle section.

The third important consequence of our simple domain-wall model is that it describes very well the gross features of the nearest-neighbor correlations $F_{\rm cor}(i)=\langle \tau_i \tau_{i+1} \rangle - \langle \tau_i \rangle \langle \tau_{i+1} \rangle$, evident from Fig. 5. Indeed, ignoring the $1/L$ corrections, we have

$$F_{\rm cor}(i) = \begin{cases} (1-2\alpha)^2[P(\xi<x)-P^2(\xi<x)] & \text{if } 0<x<1 \text{ or } 2<x<3 \\ [1-2\alpha(1-\alpha)][P(\xi<x)-P^2(\xi<x)] & \text{if } 1<x<2, \end{cases} \tag{60}$$

where $x=i/L$. Thus, by using Eq. (56) we obtain the explicit expressions for the nearest-neighbor correlation function:

$$F_{\rm cor}(i) = \begin{cases} (1-2\alpha)^2(p_1 x - p_1^2 x^2) & \text{if } 0<x<1 \\ [1-2\alpha(1-\alpha)][-2+9p_1(1-p_1)+(1-2p_1)^2(3x-x^2)] & \text{if } 1<x<2 \\ (1-2\alpha)^2[p_1(3-x)-p_1^2(3-x)^2] & \text{if } 2<x<3. \end{cases} \tag{61}$$

The above expressions describe very well the simulation results, both qualitatively and quantitatively. It can be readily checked that the maximum of the central parabola is reached at $x=3/2$ and equals $[1-2\alpha(1-\alpha)]/4 \approx 0.156$, while the left and right parabolic wings start from zero at the outer ends $x=0$ and $x=3$, respectively, and grow inward up to $(1-2\alpha)^2 p_1(1-p_1) \approx 0.040$ at the points $x=1$ and $x=2$, respectively.

Another interesting finding is the existence of strong cross correlations between sites of the two branches, $F_{\rm cross}(i) = \langle \tau_i^{(1)} \tau_i^{(2)} \rangle - \langle \tau_i^{(1)} \rangle \langle \tau_i^{(2)} \rangle$, which are almost constant and of the order 0.1 along the whole length of the middle section.

3. Case $\alpha<\beta$ and $\beta<0.5$

In this case the phase structure $(\mathcal{H},\mathcal{H},\mathcal{H})$, given by Eq. (40), was simulated with $\alpha=0.5$ and $\beta=0.25$ for chain segments of length $L=100$. The relaxation time for the bulk density was found to be $N_\tau \simeq 4\times 10^3$ SPS, and the steady-state quantities were evaluated after averaging over 300 runs of length 10^4 SPS each. The local density profile shown in Fig. 6 displays for each chain segment the features typical for a simple chain in a high-density phase. The comparison of the theoretical predictions and the simulation results for the current and the bulk densities in the simple-chain segments shows a fairly good agreement:

$$J^{\rm th}=0.1875,\ \rho_1^{\rm th}=0.75,\ \rho_{2,3}^{\rm th}=0.89528\ldots,\ \rho_4^{\rm th}=0.75,$$
$$J^{\rm sim}=0.1870(5),\ \rho_1^{\rm sim}=0.749(1).\ \rho_{2,3}^{\rm sim}=0.896(1),$$
$$\rho_4^{\rm sim}=0.7504(5). \tag{62}$$

The details of the density profiles are also well explained. The density profile of the head chain segment is typical for a simple chain in the subregion $\beta<\alpha<1/2$ of the high-density phase, where $\beta_1<1/2$ and $\beta_1<\alpha<1-\beta_1$. These conditions hold, since in the case under consideration we have $\beta_1=\beta=0.25$. From the simple-chain solution in the thermodynamic limit it follows that the density profile of C_1 is bent downward near the first site, where it starts from the value

$$\langle \tau_1 \rangle^{\rm th} = 1-\beta(1-\beta)/\alpha = 0.625. \tag{63}$$

This value is in excellent agreement with the simulation result $\langle \tau_1 \rangle^{\rm sim}=0.625(1)$.

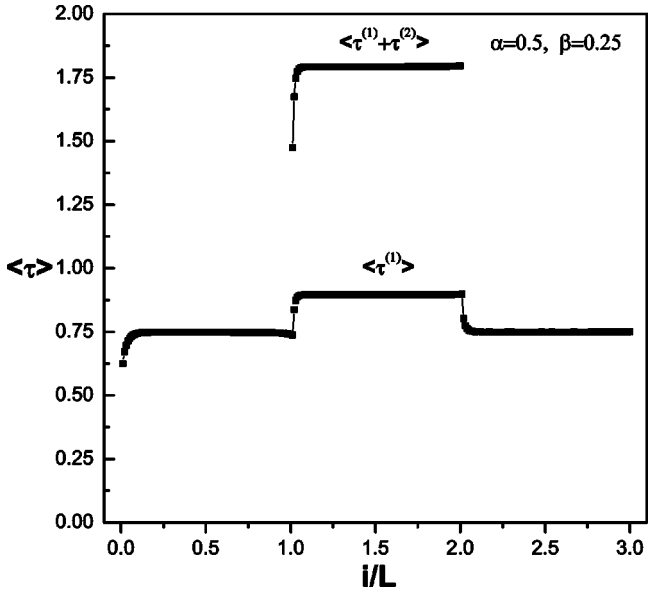

FIG. 6. Computer simulation results for the local density profile $\langle \tau \rangle$ in the system as function of the scaled distance $x=i/L$, $i=1,2,\ldots,3L$, in the high-density phase $(\mathcal{H},\mathcal{H},\mathcal{H})$ for the specific choice $\alpha=0.5, \beta=0.25$.

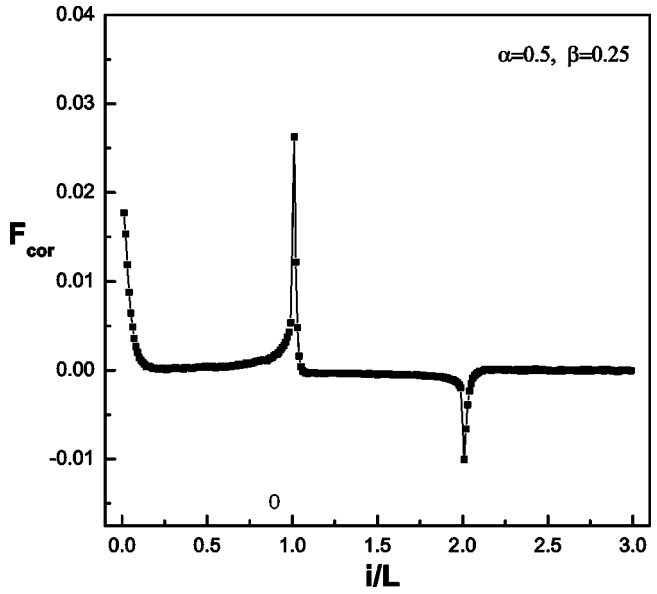

FIG. 7. The simulation results for the nearest-neighbor correlation function F_{cor} in the high density phase $(\mathcal{H},\mathcal{H},\mathcal{H})$ for the specific choice $\alpha=0.5,\beta=0.25$.

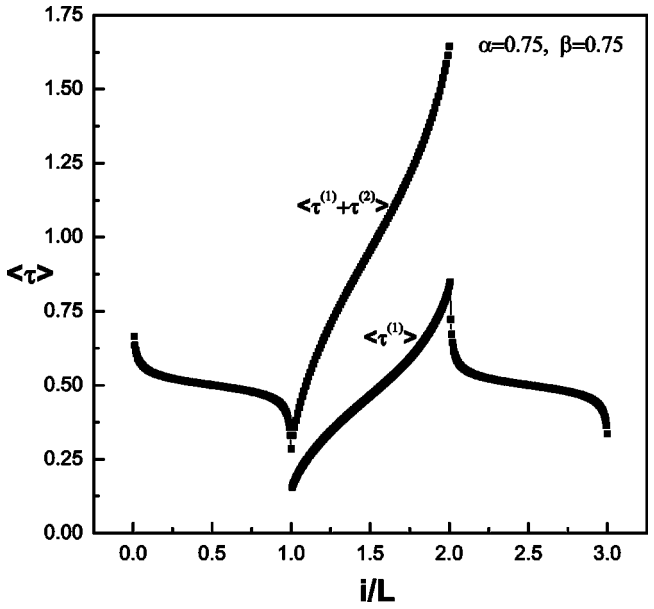

FIG. 8. The simulation results for the averaged density profile $\langle\tau\rangle$ in the system as function of the scaled distance $x=i/L$, $i=1,2,\ldots,3L$, at the phase point $\alpha=0.75,\beta=0.75$.

For the chain segments $C_{2,3}$ of the middle section we have from Eq. (39) $\beta_{2,3}<1/2$, $\alpha_{2,3}>\beta_{2,3}$ and $1-\beta_{2,3}=\rho^{+}_{2,3}(\beta)>\alpha_{2,3}$. Thus, $C_{2,3}$ are also in the subregion $\beta<\alpha<1/2$ of the high-density phase and their density profile is expected to start from the value

$$\langle\tau^{(1,2)}_{L_1+1}\rangle^{\rm th}=1-\beta_{2,3}(1-\beta_{2,3})/\alpha_{2,3}=0.6666\ldots. \quad (64)$$

This prediction of our simple theory is significantly lower than the simulation estimate $\langle\tau^{(1,2)}_{L_1+1}\rangle^{\rm sim}\approx 0.737$. The observed discrepancy can be attributed to the rather strong nearest-neighbor correlations that develop at the junction of the head chain with the double-chain middle section, see Fig. 7.

The local density profile of the tail chain segment C_4 is typical for a simple chain in the subregion $\alpha>1/2,\beta<1/2$ of the high-density phase, defined by the inequalities $\beta<1/2$, $1-\alpha_4<\beta<\alpha_4$. This is the case indeed, since Eq. (38) yields $\alpha_4>1$. The theoretical prediction for the local density at the first site of C_4 is

$$\langle\tau_{L_1+L_2+1}\rangle^{\rm th}=1-\beta(1-\beta)/\alpha_4=0.895\,28\ldots, \quad (65)$$

which is slightly lower than the simulation result $\langle\tau_{L_1+L_2+1}\rangle^{\rm sim}\approx 0.898$. This discrepancy may be due to the nearest-neighbor anticorrelations that develop at the junction of the double-chain middle section with the tail chain, see Fig. 7.

4. Case $\alpha>1/2$ and $\beta>1/2$

In this case it is the phase structure $(\mathcal{M},\mathcal{C},\mathcal{M})$ that is realized in our computer simulations out of the three possibilities given by Eqs. (47)–(49). Here we present the results for $\alpha=\beta=0.75$ and chain segments of length $L=200$. The estimated relaxation time for the bulk density in this case is $N_\tau\simeq 1.75\times 10^6$ SPS, and the steady-state quantities of interest were evaluated by averaging over 100 runs of length 5.5×10^6 each. Having in mind the eventual finite-size effects, the estimated current $J^{\rm sim}\approx 0.2518$ agrees well enough with the theoretical value $J^{\rm th}=0.25$. The local density profile is shown in Fig. 8. The head and tail chain segments display density profiles that are typical for a simple chain in the maximum-current phase. This is confirmed by the fairly good agreement of the theoretical predictions and the simulation results for the local densities at the end points of these chain segments:

$$\langle\tau_1\rangle^{\rm th}=0.666\,66\ldots,\ \langle\tau_{L_1}\rangle^{\rm th}=0.292\,89\ldots,$$
$$\langle\tau_{L_1+L_2+1}\rangle^{\rm th}=0.853\,55\ldots,\ \langle\tau_{L_{\rm tot}}\rangle^{\rm th}=0.333\,33\ldots,$$
$$\langle\tau_1\rangle^{\rm sim}\approx 0.6643,\ \langle\tau_{L_1}\rangle^{\rm sim}\approx 0.2842,$$
$$\langle\tau_{L_1+L_2+1}\rangle^{\rm sim}\approx 0.8481,\ \langle\tau_{L_{\rm tot}}\rangle^{\rm sim}\approx 0.3357. \quad (66)$$

Somewhat problematic seems the interpretation of the density profile in the chain segments of the middle section. Instead of being a straight line interpolating between the densities $\rho^{-}_{2,3}$ and $\rho^{+}_{2,3}$ of the low- and high-density phases, it shows pronounced curvatures near both ends. The comparison of our theoretical predictions and the simulation results for the local densities at the ends of the chain segments $C_{2,3}$,

$$\langle\tau^{(1,2)}_{L_1+1}\rangle^{\rm th}=0.146\,44\ldots,\ \langle\tau^{(1,2)}_{L_1+L_2}\rangle^{\rm th}=0.853\,55\ldots,$$
$$\langle\tau^{(1,2)}_{L_1+1}\rangle^{\rm sim}\approx 0.1548,\ \langle\tau^{(1,2)}_{L_1+L_2}\rangle^{\rm sim}\approx 0.8345 \quad (67)$$

shows deviations larger than the estimated statistical accuracy. A detailed analysis shows that these deviations are due to the nearest-neighbor correlations, which are not negligible

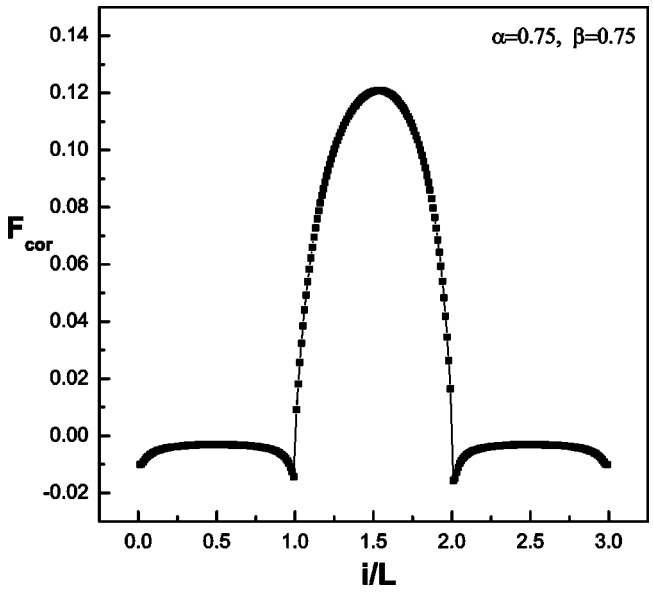

FIG. 9. The simulation results for the nearest-neighbor correlation function F_{cor} at the phase point $\alpha=0.75, \beta=0.75$.

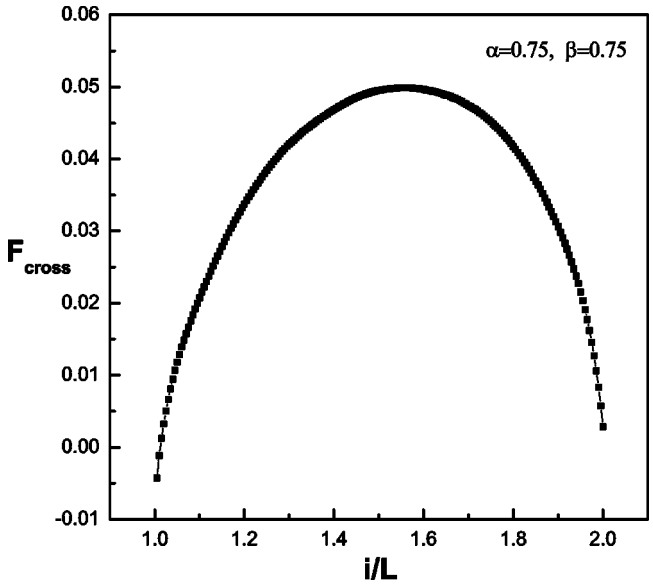

FIG. 10. The simulation results for the cross-correlation function $F_{cross}=\langle\tau_i^{(1)}\tau_i^{(2)}\rangle-\langle\tau_i^{(1)}\rangle\langle\tau_i^{(2)}\rangle$ between sites i belonging to the different branches of the loop at the phase point $\alpha=0.75, \beta=0.75$.

in the maximum-current phase. Indeed, from the exact expressions for the current along the two equivalent bonds after the bifurcation point,

$$J=(1/2)\langle\tau_{L_1}(1-\tau^{(1)}_{L_1+1})\rangle+(1/2)\langle\tau_{L_1}(1-\tau^{(2)}_{L_1+1})\rangle, \quad (68)$$

and before the merging point,

$$J=\langle\tau_{L_1+L_2}(1-\tau^{(1)}_{L_1+L_2+1})\rangle+\langle\tau_{L_1+L_2}(1-\tau^{(2)}_{L_1+L_2+1})\rangle, \quad (69)$$

we obtain the following exact relationships:

$$\langle\tau^{(1,2)}_{L_1+1}\rangle=1-[J+F_{\rm cor}(L_1)]/\langle\tau_{L_1}\rangle,$$

$$\langle\tau^{(1,2)}_{L_1+L_2}\rangle=[J/2+F_{\rm cor}(L_1+L_2)]/[1-\langle\tau_{L_1+L_2+1}\rangle]. \quad (70)$$

By inserting here the simulation estimates for the nearest-neighbor correlations $F_{\rm cor}(L_1)\approx-0.0116$ and $F_{\rm cor}(L_1)\approx0.000\,654$, and the values of the corresponding average occupation numbers given in the second line of Eq. (66), we obtain the results $\langle\tau^{(1,2)}_{L_1+1}\rangle=0.154\,77$ and $\langle\tau^{(1,2)}_{L_1+L_2}\rangle=0.8329$, which coincide with the estimates from our computer simulations within the numerical precision. The same argument holds for the last site of the head chain and the first site of the tail chain, see Eq. (66), leading to the correct values $\langle\tau_{L_1}\rangle=0.2842$ and $\langle\tau_{L_1+L_2+1}\rangle=0.8483$.

The nearest-neighbor correlations are shown in Fig. 9. Their parabolic dependence on the distance from the ends of the chain segments $C_{2,3}$ is indicative of coexistence with completely delocalized domain wall between the low- and high-density phases. In such a case, the theory predicts that the nearest-neighbor correlations attain the maximum value of $(\rho^+_{2,3}-\rho^-_{2,3})^2/4=0.125$ at the middle of the chain. An inspection of Fig. 9 shows that the above value is very close to the simulation result.

Similar to the case $\alpha=\beta=0.25$, we find rather strong cross correlations between sites with the same label i belonging to the two branches of the middle section, which is quite interesting and unexpected result of our simulations. The spatial dependence of the cross correlations is shown in Fig. 10.

V. DISCUSSION

We have studied the TASEP on a directed graph with nontrivial topology and open boundaries. The local density profiles, nearest-neighbor correlations along the chain segments, and cross correlations between equivalent sites belonging to the two branches of the middle section were simulated for values of the parameters α and β which correspond to all the phases of a simple chain. The presence of a double-chain middle section leads in some of the cases to expected steady-state phase structures, such as $(\mathcal{L},\mathcal{L},\mathcal{L})$ and $(\mathcal{H},\mathcal{H},\mathcal{H})$, where $\mathcal{L}$ and $\mathcal{H}$ stand for low- and high-density phases, respectively, which are characterized by short-range correlations appearing in the neighborhood of the bifurcation and merging sites of the network. Otherwise, the properties of the simple-chain segments are close to those expected on the grounds of the approximation which ignores the above mentioned correlations. For example, the reduction of the current by factor of $1/2$ in the equivalent branches of the middle section leads to a radical decrease, or increase, of the bulk density in the $(\mathcal{L},\mathcal{L},\mathcal{L})$ and $(\mathcal{H},\mathcal{H},\mathcal{H})$ cases, respectively.

Rather unexpected are the observed $(\mathcal{M},\mathcal{C},\mathcal{M})$ and what we would call mixed $(\mathcal{L},\mathcal{C},\mathcal{H})$ and $(\mathcal{C},\mathcal{C},\mathcal{C})$ phase structures.

In the former case, which takes place when $\alpha > 1/2$ and $\beta > 1/2$, the bending in opposite directions of the local density profile of the head and tail chains in the maximum-current phase leads to a coexistence of low- and high-density phases in the chain segments of the middle section. The latter case occurs at $\alpha = \beta < 1/2$ when a simple chain is on the coexistence line. For our chain with a double-chain middle section we have found clear evidence of a delocalized domain wall which has different probabilities of being found in the head/tail chains and in the branches of the middle section. No theoretical explanation has been found yet for the significant cross correlations between the random occupation numbers of equivalent sites belonging to the two branches of the middle section whenever these branches are in a coexistence phase.

In all the cases studied, the current through the chain with a double-chain middle section was found to be the same (within statistical error) as the one through a simple chain under the same injection and removal rates.

To illustrate the effect of the double-chain section, we compare the fundamental diagrams, flow versus density, in our case and in the case of a simple chain, see Fig. 11. The most remarkable effects are the appearance of a plateau at the maximum current and the existence of densities greater than unity. To explain the latter feature one has to take into account that, in contrast to the simple-chain case, in our network the bulk density happens to be inhomogeneous. The total bulk density is defined as $\rho = (1/3)\Sigma_{i=1}^{4} \rho_i$, and the fundamental diagram is calculated as follows: its left-hand half is obtained under fixed $\beta = 0.75$, varying $\alpha \in (0,1)$, and its right-hand half under fixed $\alpha = 0.75$, varying $\beta \in (0,1)$. Remarkably, on going deeper into the maximum-current phase along any of the above paths, the total density of the middle section increases steadily, while the current stays at its maximum value, and the bulk densities in the head and tail segments remain constant, too. Since the total density $\rho_2 + \rho_3$ in the two branches of the double-chain section can exceed unity, see Fig. 6, the total bulk density exceeds unity, too. The plateau is due to the above mentioned increase of the total density at constant current. Note that the mirror symmetry with respect to the middle of the density range is preserved due to the particle-hole symmetry.

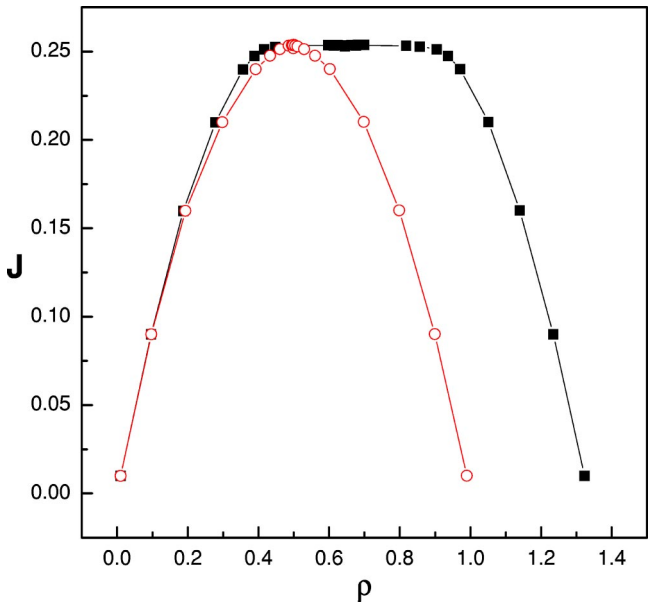

FIG. 11. (Color online) The fundamental diagram, current J vs density ρ, from the numerical simulations: the solid squares–solid line curve is the result for the system with a double-chain section in the middle; the empty circles–solid line curve is for a simple chain.

We believe that future investigations on traffic models of complicated single-lane networks are necessary and will reveal new features which have no direct analogs in the simple-chain case. Our preliminary simulations show that some of the observed correlation effects depend strongly on the length of the head and chain segments.

[1] C. T. MacDonald, J. H. Gibbs, and A. C. Pipkin, Biopolymers **6**, 1 (1968).
[2] F. Spitzer, Adv. Math. **5**, 246 (1970).
[3] J. Krug, Phys. Rev. Lett. **67**, 1882 (1991).
[4] B. Derrida, E. Domany, and D. Mukamel, J. Stat. Phys. **69**, 667 (1992).
[5] G. Schütz and E. Domany, J. Stat. Phys. **72**, 277 (1993).
[6] B. Derrida, M. R. Evans, V. Hakim, and V. Pasquier, J. Phys. A **26**, 1493 (1993).
[7] N. Rajewsky, A. Schadschneider, and M. Schreckenberg, J. Phys. A **29**, L305 (1996).
[8] A. Honecker and I. Peschel, J. Stat. Phys. **88**, 319 (1997).
[9] H. Hinrichsen, J. Phys. A **29**, 3659 (1996).
[10] N. Rajewsky and M. Schreckenberg, Physica A **245**, 139 (1997).
[11] M. R. Evans, N. Rajewsky, and E. R. Speer, J. Stat. Phys. **95**, 45 (1999).
[12] J. de Gier and B. Nienhuis, Phys. Rev. E **59**, 4899 (1999).
[13] J. Brankov and N. Pesheva, Phys. Rev. E **63**, 046111 (2001).
[14] S. A. Janovsky and J. L. Lebowitz, Phys. Rev. A **45**, 618 (1992).
[15] F. H. Jafarpour, J. Phys. A **33**, 8673 (2000).
[16] P. F. Arndt, T. Heinzel, and V. Rittenberg, J. Phys. A **31**, 833 (1998).
[17] V. Karimipour, Europhys. Lett. **47**, 304 (1999).
[18] G. M. Schütz, in *Phase Transitions and Critical Phenomena*, edited by C. Domb and J. L. Lebowitz (Academic Press, London, 2001), Vol. 19.
[19] D. Helbing, Rev. Mod. Phys. **73**, 1067 (2001).
[20] K. Nagel and M. Schreckenberg, J. Phys. I **2**, 2221 (1992).
[21] M. Schreckenberg, A. Schadschneider, K. Nagel, and N. Ito, Phys. Rev. E **51**, 2939 (1995).
[22] M. M. Pedersen and P. T. Ruhoff, Phys. Rev. E **65**, 056705 (2002).
[23] R. Jiang, Q.-S. Wu, and B.-H. Wang, Phys. Rev. E **66**, 036104 (2002).

[24] V. Popkov, L. Santen, A. Schadschneider, and G. M. Schütz, J. Phys. A **34**, L45 (2001).
[25] K. Nagel, D. E. Wolf, P. Wagner, and P. Simon, Phys. Rev. E **58**, 1425 (1998).
[26] O. Biham, A. A. Middleton, and D. Levine, Phys. Rev. A **46**, R6124 (1992).
[27] T. Nagatani, J. Phys. A **198**, 108 (1993).
[28] S.-i. Tadaki and M. Kikuchi, Phys. Rev. E **50**, 4564 (1994).
[29] T. Nagatani, Phys. Rev. E **48**, 3290 (1993).
[30] S.-i. Tadaki, Phys. Rev. E **54**, 2409 (1996).
[31] A. Benyoussef, H. Chakib, and H. Ez-Zahraouy, Phys. Rev. E **68**, 026129 (2003).